HHS Public Access

Author manuscript

Sci Signal. Author manuscript; available in PMC 2020 May 13.

Published in final edited form as:

Sci Signal. ; 12(603): . doi:10.1126/scisignal.aaw9315.

Developmentally regulated KCC2 phosphorylation is essential for dynamic GABA-mediated inhibition and survival

Miho Wantanabe[1,#], **Jinwei Zhang**[2,#], **M. Shahid Mansuri**[3,#], **Jingjing Duan**[4], **Jason K. Karimy**[3], **Eric Delpire**[5], **Seth L. Alper**[6], **Richard P. Lifton**[7], **Atsuo Fukuda**[1,8,*], **Kristopher T. Kahle**[9,*]

[1]Department of Neurophysiology, Hamamatsu University School of Medicine, Hamamatsu, Shizuoka 431-3192, Japan

[2]Institute of Biomedical and Clinical Sciences, Medical School, College of Medicine and Health, University of Exeter, Hatherly Laboratories, Exeter, EX4 4PS, UK

[3]Department of Neurosurgery, Yale School of Medicine, New Haven, CT 06510, USA

[4]Human Aging Research Institute, School of Life Sciences, Nanchang University, Nanchang, Jiangxi, 330031, China

[5]Department of Anesthesiology, Vanderbilt University School of Medicine, Nashville, TN 37232, USA

[6]Division of Nephrology, Department of Medicine, Beth Israel Deaconess Medical Center and Harvard Medical School, Boston, MA 02215, USA; and The Broad Institute of Harvard and the Massachusetts Institute of Technology, Cambridge, MA 02139, USA

[7]Laboratory of Human Genetics and Genomics, The Rockefeller University, New York, New York, USA; Department of Genetics, Yale University School of Medicine, New Haven, CT 06511, USA

[8]Advanced Research Facilities and Services, Preeminent Medical Photonics Education and Research Center, Hamamatsu University School of Medicine, Hamamatsu, Shizuoka 431-3192, Japan

[9]Departments of Neurosurgery, Pediatrics, and Cellular and Molecular Physiology; Centers for Mendelian Genomics, Yale School of Medicine, New Haven, CT 06510, USA

Abstract

Despite its importance for γ-aminobutyric acid (GABA) inhibition and involvement in neurodevelopmental disease, the regulatory mechanisms of the K^+/Cl^- co-transporter KCC2 (encoded by *SLC12A5*) during maturation of the central nervous system (CNS) are not entirely

*Corresponding authors. kristopher.kahle@yale.edu (K.T.K.); axfukuda@hama-med.ac.jp (A.F.).
#These authors contributed equally

Author contributions: K.T.K., M.W., J.Z., M.S.M., and A.F. conceived and designed the experiments. M.W., J.Z., M.S.M., J.D., J.K.K., E.D., S.L.A., R.P.L., A.F., and K.T.K. performed the experiments. J.Z., M.W., M.S.M., A.F., and K.T.K. analyzed the data. J.Z., M.W., M.S.M., A.F., and K.T.K. wrote the manuscript.

Competing interests: The authors declare that they have no competing interests.

Data and materials availability: All data needed to evaluate the conclusions in the paper are present in the paper or the Supplementary Materials.

understood. Here, we applied quantitative phosphoproteomics to systematically map sites of KCC2 phosphorylation during CNS development in the mouse. KCC2 phosphorylation at Thr^{906} and Thr^{1007}, which inhibits KCC2 activity, underwent dephosphorylation in parallel with the GABA excitatory-inhibitory sequence in vivo. Knock-in mice expressing the homozygous phospho-mimetic KCC2 mutations T906E/T1007E ($Kcc2^{E/E}$), which prevented the normal developmentally regulated dephosphorylation of these sites, exhibited early postnatal death from respiratory arrest and a marked absence of cervical spinal neuron respiratory discharges. $Kcc2^{E/E}$ mice also displayed disrupted lumbar spinal neuron locomotor rhythmogenesis and touch-evoked status epilepticus associated with markedly impaired KCC2-dependent Cl^- extrusion. These data identify a previously unknown phosphorylation-dependent KCC2 regulatory mechanism during CNS development that is essential for dynamic GABA-mediated inhibition and survival.

INTRODUCTION

Type A GABA receptors ($GABA_A$Rs) are ligand-gated anion channels that allow bidirectional flux of Cl^- ions. The direction of net Cl^- flux, governed by the transmembrane electrochemical gradient for Cl^-, is determined by regulation of the intracellular concentration of Cl^- ions $[Cl^-]_i$ and the post-synaptic membrane potential (1). $GABA_A$R activation in the adult CNS triggers hyperpolarizing phasic and tonic inhibitory neurotransmission. In contrast, $GABA_A$R activation in the immature CNS elicits inhibitory shunting of membrane conductance or even increased membrane excitability, which plays an important role in brain development via effects on neuronal proliferation, migration, and synaptogenesis (2–7).

The developmental “switch” in GABA function from excitatory to inhibitory has been attributed to a transition from the immature neuronal $[Cl^-]_i$ of ~15 to 20 mM to the mature neuronal value of ~4 mM (8). This transition requires increased neuronal Cl^- extrusion dependent on the K-Cl cotransporter KCC2 (*SLC12A5*), beginning in rodents during the first postnatal week and progressing through the brain in a caudal-to-rostral direction (8–10). KCC2-null mice with increased levels of neuronal $[Cl^-]_i$ die perinatally and exhibit anomalous GABA-mediated neuronal excitation (11). Neuronal hyperexcitability induced by KCC2 hypofunction promotes epilepsy, autism, and other neurodevelopmental pathologies (12).

The critical role of KCC2 in GABA signaling and neurological disease has generated considerable interest in its mechanisms of regulation. Although the total abundance of KCC2 increases along with the GABA excitation-to-inhibition transition, the relative contributions to the developmental increase in KCC2 activity of altered KCC2 polypeptide abundance and altered regulation of KCC2 activity remain unclear. Moreover, some neurons of the brainstem, spinal cord, and suprachiasmatic nucleus dynamically modulate $[Cl^-]_i$ such that GABA rhythmogenically cycles from excitatory to inhibitory effects in respiratory (13), locomotor (14), and circadian networks (15).

KCC2 phosphorylation alters its activity, regulates neuronal $[Cl^-]_i$, and strongly impacts the GABA reversal potential (E_{GABA}) (8, 16–22). Nonetheless, the sites of regulated phosphorylation in KCC2 have not been systematically identified nor functionally examined

during CNS development in vivo. Among identified phospho-sites, the dual phosphorylation of Thr^{906}/Thr^{1007} ("$pThr^{906}/pThr^{1007}$") is a particularly potent switch of KCC2 activity in vitro (19, 23–25). Indeed, constitutive dephosphorylation of KCC2 Thr^{906}/Thr^{1007}, achieved via alanine mutagenesis at these sites, potently stimulates KCC2 activity > 10-fold (24). KCC2 $pThr^{906}/pThr^{1007}$ maintains the GABA-dependent depolarization of cultured immature neurons by reducing neuronal Cl^- extrusion capacity (24, 26, 27). However, the function of the KCC2 $pThr^{906}/pThr^{1007}$ phospho-switch has not been examined during CNS development in vivo.

In this study, we tested the hypothesis that regulated phosphorylation of KCC2, specifically at the WNK/SPAK-kinase-regulated Thr^{906}/Thr^{1007} phosphorylation sites of KCC2, is essential for normal CNS function and organismal survival. To test this hypothesis, we performed unbiased quantitative phospho-proteomics to systematically map sites of KCC2 phosphorylation during development. We also performed detailed biochemical and electrophysiological characterization of a novel mouse model of KCC2 that mimics constitutive phosphorylation at $pThr^{906}/pThr^{1007}$ through glutamic acid mutagenesis.

RESULTS

Systematic identification of KCC2 phosphorylation sites during development

KCC2 expression is limited to neurons in the central nervous system (CNS) (28). To map potential sites of KCC2-regulated phosphorylation in vivo during CNS development, we immunoprecipitated endogenous KCC2 from E18.5, P0, P20, and adult mouse brains using specific anti-KCC2 antibodies, and fractionated the purified immune complexes by sodium dodecyl sulphate-polyacrylamide gel electrophoresis (SDS-PAGE) (see Methods; Fig. 1A). KCC2 samples were then digested with trypsin, and the resulting peptides identified by liquid chromatography and dual mass spectroscopy (LC-MS/MS) (Fig. 1B). Phospho peptides and specific phosphorylation sites were assigned by precise match of predicted and observed m/z ratios of precursor ions and their product fragment ions using MaxQuant (29, 30).

Eighteen independent KCC2 phosphorylation sites were reproducibly identified at all time points in three independent experiments (Fig. 1C and table S1). Six sites mapped to the KCC2 intracellular amino (N)-terminal domain, three were located in the large KCC2 extracellular loop, and nine were positioned in the KCC2 intracellular carboxyl-terminal domain. Sites identified (numbering standardized to the human KCC2b isoform herein) included Thr^{906} and Thr^{1007} phosphorylated by the WNK-SPAK kinases in vitro (25); Ser^{940} phosphorylated by PKA and PKC in vitro (21, 31); and Thr6 phosphorylated by SPAK/OSR1 in vitro (25). Candidate kinases for other identified sites in the KCC2 N-terminus included PKA, PKC, CAMK2, CDK5, and GSK3 (table S2). The phosphorylation sites at Ser^{25}, Ser^{31}, Ser^{937}, Ser^{1025}, and Ser^{1026} did not match defined kinase specificity motifs. Three previously unknown phosphorylation sites detected in KCC2, Thr^{8}, Thr^{799} and Ser^{812}, were not previously annotated in the mouse PhosphoSitePlus database (32).

Potential developmentally regulated phospho-sites were determined by label-free quantitation based on normalized peptide intensities (30). Among the 18 distinct KCC2

phosphorylation sites (table S1), phosphorylation at 8 sites changed significantly during development, as assessed at E18.5, P0, P20, and adult (Fig. 1D). Hierarchical clustering analysis showed two distinct clusters of developmentally regulated phosphorylation sites (Fig. 1D). In the first cluster, Ser^{932}, Thr^{999}, and Ser^{1026} showed increased phosphorylation during development. A second cluster containing Thr^{6}, Thr^{8}, Thr^{906}, Ser^{1022}, and Ser^{1025} showed decreased phosphorylation during development. Among all identified sites, Thr^{906} showed the greatest reduction in developmental phosphorylation among all KCC2 phosphorylation sites (>65% reduction in adult brain vs. E18.5 brain; Fig. 1D).

KCC2 phosphorylation sites Thr^{906} and Thr^{1007} were of particular interest, as these KCC2 residues are highly phosphorylated during early CNS development, are evolutionarily conserved from frogs to humans (fig. S1, A and B) and all human KCC paralogs (fig. S1C), and are critical regulators of KCC2 activity (23). We therefore assessed KCC2 phosphorylation at these sites in the developing brain by anti-KCC2 immunoblot of immunoprecipitates with phospho-specific antibodies recognizing p-Thr^{906} and p-Thr^{1007}, as described previously (19, 25) (Fig. 1E). In wild-type (WT) mouse brains, KCC2 phosphorylation at Thr^{906} and Thr^{1007} decreased >95% during CNS development from E18.5 to adult, in parallel with a >340% increased KCC2 abundance (Fig. 1E) (24).

An in vivo genetic model to prevent the developmental dephosphorylation of KCC2 at Thr^{906}/Thr^{1007}

To investigate the in vivo role of regulated KCC2 pThr^{906}/pThr^{1007} during CNS development, we used homologous recombination to generate knock-in mice expressing the dual KCC2 glutamic acid substitutions T906E/T1007E (“T906E/T1007E”, Fig. 2A), which antagonizes KCC2-dependent Cl^- extrusion from neuronal cells in vitro by mimicking inhibitory phosphorylation at these sites (24, 27, 33). Southern blot analysis (fig. S2A) and DNA sequencing confirmed the presence of the T906E and T1007E mutations at their respective codons in KCC2 exons 22 and 24 (Fig. 2B).

Heterozygous KCC2 T906E/T1007E$^{+/wt}$ mutants were viable, fertile, and survived to adulthood without apparent abnormalities, as true also for heterozygous and homozygous KCC2 T906A/T1007A mice (34). Among progeny from *T906E/T1007E*$^{+/wt}$ intercrosses, homozygous *T906E/T1007E*$^{+/+}$ mutant mice (herein termed “*Kcc2*$^{E/E}$” mice) developed in utero at the expected Mendelian ratio, whereas all *Kcc2*$^{E/E}$ died within 4 to 12 hours after birth due to spontaneous cessation of regular respiratory rhythm (Fig. 2C).

Pregnant mice were therefore subjected to Caesarian section at gestational day 18.5 (E18.5). WT and heterozygous pups consistently survived this early delivery and exhibited similar postnatal courses. *Kcc2*$^{E/E}$ neonates were grossly normal, though 11.3% lower in body weight than WT or *T906E/T1007E*$^{+/wt}$ mice (fig. S2B). P0 *Kcc2*$^{E/E}$ mice had anatomically and histologically normal brain, heart, lungs, and other organs (Fig. 2D and fig. S3). Whereas *T906E/T1007E*$^{+/wt}$ and *Kcc2*$^{E/E}$ brain tissues exhibited the expected decreases in anti-KCC2 pThr^{906} and pThr^{1007} phospho-specific antibody immuno-reactivity (27) (Fig. 2E and fig. S2C), the total polypeptide abundances of KCC2, NKCC1, and the NKCC1/KCC2 regulatory kinases WNK1/SPAK were unchanged (Fig. 2E and fig. S2C).

Touch-provoked recurrent generalized seizures in *Kcc2*$^{E/E}$ mice

Reduction of KCC2 activity increases neuronal $[Cl^-]_i$, compromises GABAergic inhibition, and promotes spontaneous, recurrent generalized seizures in mice and humans (35). Strikingly, *Kcc2*$^{E/E}$, but not WT or *T906E/T1007E*$^{+/wt}$, mice exhibited severe, touch-provoked, recurrent generalized seizures triggered by (i) mild brush stroke (Fig. 2, F to H, and movie S1), (ii) tail pinch (Fig. 2, I to K, and movie S2), and (iii) tail suspension (Fig. 2, L to N, and movie S3). Brush stroke induced generalized tonic-clonic seizures of >55s duration, including tonic convulsions with or without opisthotonus (Fig. 2, F to H). Tail pinch provoked primary or secondary generalized tonic-clonic seizures of >32s duration, and tonic convulsions with or without opisthotonus (Fig. 2, I to K). Tail suspension uniformly elicited severe generalized tonic primary or secondary convulsions with opisthotonus (Fig. 2L–N). *Kcc2*$^{E/E}$ mice also exhibited spontaneous seizures (movie S4), increasing in frequency before death.

An anomalous neuronal distribution with normal dendritic spine morphology in *Kcc2*$^{E/E}$ brains

KCC2-mediated K^+-Cl^- cotransport is required for GABA-dependent neuronal proliferation and migration (36). We therefore examined the neuronal distribution (reflecting both neuronal proliferation and migration) in the developing *Kcc2*$^{E/E}$ mouse brain by labeling neurons with 5-ethynyl-2′-deoxyuridine (EdU) at E14.5, followed by counting at E18.5 (Fig. 3A). Analysis revealed fewer EdU-labeled neurons in the *Kcc2*$^{E/E}$ septum, greater numbers of EdU-labeled neurons in preoptic areas (POA), and unchanged numbers of EdU-labeled neurons in caudate putamen and deeper neocortex (Fig. 3B).

Independent of its Cl^- transport function, KCC2 regulates dendritic spine maturation and excitatory synapse development via structural interactions between KCC2 and the spine cytoskeleton (37). We therefore assessed neuronal (and dendritic spine) morphology in primary cultures of cortical neurons from Kcc2E/E mice. Soma size and shape, dendritic arborization, and spine morphogenesis were similar in day 26 primary cultured WT and *Kcc2*$^{E/E}$ neurons (Fig. 3C).

Impaired GABA-dependent Cl^- extrusion capacity of *Kcc2*$^{E/E}$ neurons

During development, KCC2 becomes the dominant mediator of Cl^- extrusion in CNS neurons (8). Deficits in KCC2-mediated Cl^- extrusion result in increased $[Cl^-]_i$, and this facilitates pathological $GABA_A$R-mediated depolarizing responses (38). The abundance of KCC2 at P0 is greater in the spinal cord than in the neocortex or hippocampus (17, 18, 20, 39). Therefore, we applied the gramicidin-perforated patch-clamp technique in ventral spinal cord neurons and in acute lumber spinal cord slices from P0 WT and *Kcc2*$^{E/E}$ mice (Fig. 4A) to measure the GABA reversal potential (E_{GABA}), determined primarily by the Cl^- equilibrium potential (reflecting $[Cl^-]_i$ (9, 40) and an index of KCC2 activity) (11). E_{GABA} was indistinguishable in WT and *Kcc2*$^{E/E}$ mice spinal cord neurons (Fig. 4B). To measure efficacy of KCC2 mediated Cl^- extrusion, we performed transient Cl^- loading by whole-cell patch-clamp recording using a low Cl^- (12 mM) pipette solution. Ventral spinal cord neurons Cl^--loaded by GABA during depolarizing voltage-clamp underwent current clamp recording of GABA responses at 20 s intervals over a 5 min period (41). In Cl^--loaded

conditions, GABA-evoked potentials in WT spinal cord neurons increased >4-fold (Fig. 4C), reflecting increased $[Cl^-]_i$, then rapidly relaxed to initial amplitudes, consistent with rapid KCC2-dependent Cl^- extrusion (Fig. 4C). Whereas WT peak potentials had fully recovered to initial values within 100 s after prolonged GABA exposure, *Kcc2*$^{E/E}$ peak potentials remained >20% above initial values (Fig. 4D).

Lack in spontaneous respiratory discharge recordings from ventral cervical spinal cord neurons of *Kcc2*$^{E/E}$ mice

Because *Kcc2*$^{E/E}$ mice died in respiratory distress shortly after birth, we examined the effects of the KCC2 T906E/T1007E mutation on spontaneous respiratory discharge. Respiratory discharges were recorded from C4 or C5 ventral cervical spinal cord neurons in brainstem-spinal cord preparations (42); for further details, see the Methods). Respiratory discharges were indistinguishable in WT and heterozygous *T906E/T1007E*$^{+/wt}$ mice (Fig. 4, E and F). In contrast, spontaneous respiratory discharges were essentially absent in almost all homozygous *Kcc2*$^{E/E}$ mice (Fig. 4, E and F). A single *Kcc2*$^{E/E}$ mouse showed abnormal bursting activity (21 min^{-1}) and one other *Kcc2*$^{E/E}$ mouse showed infrequent breathing (1 min^{-1}). These results suggest that the abnormal respiratory patterns preceding death in *Kcc2*$^{E/E}$ mice result from aberrant spontaneous respiratory discharges in cervical spinal cord neurons.

Altered locomotor rhythm recordings from lumbar spinal cord ventral roots of *Kcc2*$^{E/E}$ mice

Analogous to the role of GABA in respiratory rhythmogenesis, the strength of GABA inhibition is an essential factor for normal locomotor rhythm (43, 44). As impaired KCC2-dependent Cl^- extrusion was observed in ventral spinal cord neurons of *Kcc2*$^{E/E}$ mice (Fig. 4, C and D), we assessed the effect of in vivo KCC2 T906E/T1007E mutation on recorded rhythmic motor activity from L2 ventral roots (Fig. 4G). Perfusion of 5-hydroxytryptamine (5-HT) induced rhythmic bursts in both WT and *T906E/T1007E*$^{+/wt}$ mice, as also previously described (45, 46). In contrast, although locomotor rhythm was observed in *Kcc2*$^{E/E}$ mice, the frequency of locomotor rhythm was significantly lower in *Kcc2*$^{E/E}$ mice than in WT and *T906E/T1007E*$^{+/wt}$ heterozygous mice (Fig. 4H). The coefficient of variation of the interburst intervals was also significantly lower in *Kcc2*$^{E/E}$ mice than in WT and *T906E/T1007E*$^{+/wt}$ mice (Fig. 4I). These results confirm that regulated KCC2 Thr^{906}/Thr^{1007} phosphorylation is essential for generation of normal locomotor rhythm.

DISCUSSION

We have shown the inhibitory phosphorylation of the WNK/SPAK-regulated Thr^{906}/Thr^{1007} motif in KCC2 is significantly reduced during the course of CNS development. Second, regulated KCC2 Thr^{906}/Thr^{1007} phosphorylation is essential for mouse survival; antagonizing the normal developmental down-regulation of KCC2 Thr906/Thr1007 via homozygous phospho-mimetic mutagenesis of these sites causes respiratory arrest and early post-natal death. Third, corroborating and extending previous in vitro findings (24, 26), phospho-mimetic mutation of Thr^{906}/Thr^{1007} in vivo prevents KCC2 from dynamically increasing its Cl^- extrusion capacity (such as in response to a Cl^- load). This results in an

imbalance of neuronal excitation and inhibition that leads to impaired rhythmogenesis in respiratory and locomotor networks, accompanied by profound neuronal hyperexcitability manifesting as touch-evoked generalized seizures. Fourth, *Kcc2*$^{E/E}$ mice exhibit anomalous neuronal distribution with normal dendritic spine morphology, consistent with the known importance of KCC2 function on neuronal proliferation and migration (47), and the activity-independent role of KCC2 in dendrite spine maturation (37, 48).

KCC2 mRNA expression in mice starts as early as E10.5 in spinal cord and brainstem, which exhibit the earliest development of KCC2-dependent Cl^- extrusion. Mouse KCC2 transcripts are expressed in developing motoneurons in spinal cord ventral horn and in medulla as early as E12.5 (11) and in sensory nuclei at E15.5, with progressively increasing expression during embryonic development (17). After E15.5, NKCC1 abundance decreases in motoneurons while KCC2 functional expression increases and contributes to emergence of a more negative E_{Cl}, so that GABA and glycine function as inhibitory neurotransmitters in the majority of mouse spinal motoneurons by E17.5 (49). This switch may correspond to the period at which locomotor networks start to generate alternating flexor and extensor motor activities, concomitant to network expression of left-right alternation, indicative of functional network inhibition (18, 50). Inhibitory spinal interneurons are essential for generation of locomotor rhythms (44). Consistent with the importance of KCC2 Thr^{906}/Thr^{1007} phosphorylation in the developmental regulation of KCC2-dependent Cl^- homeostasis, spinal cord neurons of *Kcc2*$^{E/E}$ mice exhibited a significantly impaired Cl^- extrusion capacity compared to their counterparts. The significantly impaired (slow) locomotor rhythms in *Kcc2*$^{E/E}$ mice suggest that regulated phosphorylation of KCC2 at Thr906/Thr1007 is essential for the generation of locomotor rhythm.

GABA also critically regulates respiratory rhythmogenesis and motor output patterning (51–54) and plays essential roles in termination of both inspiratory and expiratory phases of respiration (55–59). Application of the $GABA_AR$ agonist, muscimol, increased respiration-related rhythmic activities in an E17 rat brainstem-spinal cord preparation but decreased those activities in an E20 preparation (60), suggesting that GABA switches from facilitating to inhibiting respiration-related rhythmic activities during development. This GABA-induced switch in respiration-related rhythmic frequency has been attributed to a developmental decrease in $[Cl^-]_i$ (50). We showed that *Kcc2*$^{E/E}$ mice died from respiratory distress within hours after birth and lacked spontaneous respiratory discharge recordings from cervical ventral roots. These results suggest that KCC2-dependent Cl^- extrusion capacity is essential for spontaneous respiratory discharges as previously observed (11), and that KCC2 Thr906/Thr1007 phosphorylation is likely essential for developmental switches in GABA-regulated rhythmic respiration. This is compatible with the previous observation that application of a KCC2 inhibitor significantly decreased the frequency of respiration-related rhythmic activities of mice at P1 (61).

Kcc2$^{E/E}$ mice showed normal organogenesis and the developmental up-regulation of KCC2 total protein abundance. However, *Kcc2*$^{E/E}$ mouse brains exhibited significant abnormalities in neuronal distribution in the septum, hypothalamus, hippocampus, and cortex. These results suggest that regulated KCC2 Thr^{906}/Thr^{1007} phosphorylation is essential for neuronal proliferation and/or migration in developing forebrain. Considering that KCC2 is absent but

NKCC1 is highly expressed in the neuroepithelium (20, 62), altered distributions of proliferating cells might be due to disturbed migration rather than to altered proliferation. GABA is involved in radial and tangential migration of cortical cells. $GABA_A$ receptor activation is a stop signal for radial migration in the cortical plate. In contrast, depolarizing GABA promotes tangential migration of interneurons, whereas increased KCC2 expression reduces interneuron motility (63). Depolarizing GABA responses are required in immature migrating cells, because voltage-dependent Ca^{2+} channel-mediated Ca^{2+} signaling is closely coupled with migration. Thus, perturbation of immature Cl^- homeostasis in *Kcc2*$^{E/E}$ mice could result in anomalous migration. Indeed, overexpression of mutant KCC2 has been shown to arrest radial migration (26).

Status epilepticus (SE) is defined as a continuous seizure of long duration, or recurrent seizures occurring in close temporal proximity without full inter-ictal recovery. An imbalance of excitatory and inhibitory neurotransmission that results in hyperexcitation of neural network activity plays a critical role in generation of SE (68, 69). GABAergic mechanisms are critical in terminating seizures (70–73). Susceptibility to SE is higher in neonates than in adults likely reflecting depolarizing GABA functions secondary to KCC2 functional immaturity. An acute Cl^- overload due to intense neuronal activity would also reduce efficacy of GABAergic inhibition (70). In this setting, KCC2-mediated Cl^- extrusion is considered crucial for preventing rundown of GABAergic inhibition.

Gramicidin patch-clamp measurements of E18.5 neurons in WT and *Kcc2*$^{E/E}$ mice showed equivalent E_{GABA}, indicating that the transporter activity was not completely eliminated in *Kcc2*$^{E/E}$ mice. Thus, resting $[Cl^-]_i$ in the absence of increased network activity, particularly GABAergic interneuron activity, was not significantly altered in *Kcc2*$^{E/E}$ mice. However, an impairment of neuronal Cl^- extrusion velocity became evident after acute Cl^- loading. Previous reports showed that strong activation of GABAergic input can substantially increase $[Cl^-]_i$, indicating that Cl^- extrusion capacity of KCC2 is transiently overwhelmed by acute massive Cl^- influx (70, 74, 75). Thus, rapid KCC2-mediated Cl^- extrusion is required for recovery from such acute increases in $[Cl^-]_i$. The Cl^- extrusion velocity of *Kcc2*$^{E/E}$ might be lower than that of WT, explaining our observed increase in time required to reverse $[Cl^-]_i$ after its transient GABA-induced increase.

KCC2 is important not only for maintenance of static $[Cl^-]_i$ but also for recovery from transient increases in $[Cl^-]_i$ that occur during the course of repeated inhibitory inputs. Indeed, mice with mutations that prevent KCC2 Ser^{940} phosphorylation (S940A) exhibit E_{GABA} comparable to that of WT, but show a deficit in Cl^- extrusion after Cl^- loading, with increased susceptibility to kainate-induced seizures (16). *Kcc2*$^{E/E}$ mice are similarly prone to stimulus-evoked seizures. All *Kcc2*$^{E/E}$ mice exhibited SE-like tonic spasms provoked by mild sensory stimulation such as brushing (tactile), tail pinch (pain), and tail-suspension (proprioceptive and vestibular). Thus, “robust” GABAergic inhibition is required to prevent recruitment of excitation culminating in seizure propagation and extending to development of SE. Therefore, the impairment in Cl^- extrusion resulting from mild KCC2 hypofunction in *Kcc2*$^{E/E}$ mice contributes to epileptogenesis induced by activation of afferent pathways that include GABAergic inputs. Indeed, heterologous expression of two KCC2 mutants, causative for epilepsy of infancy with migrating focal seizures mimicking the patient status,

resulted in $[Cl^-]_i$ significantly higher than that associated with wild type KCC2, but lower than in the absence of KCC2. These findings clearly indicate that even mildly impaired neuronal Cl^- extrusion can significantly compromise the robustness of GABAergic inhibition in SE (40).

Our findings are also consistent with the recent demonstration that genetic mutation of KCC2 Thr^{906}/Thr^{1007} to alanine (Ala), modeling constitutive dephosphorylation, elicited enhanced KCC2 activity while limiting onset and severity of seizures in homozygous mice (34). These KCC2 T906E(A)/T1007E(A) transgenic animals together represent valuable models to study the in vivo roles of regulated KCC2 phosphorylation and provide important genetic evidence that drug development targeting the KCC2 Thr^{906}/Thr^{1007} phospho-switch is a compelling novel strategy to modulate GABA-mediated neurotransmission. Our study also identified several previously unknown candidate regulators of KCC2 Thr^{906}, such as GSK3 kinase beta, implicated in regulation of the WNK-SPAK signaling pathway (76). Our ongoing, systematic identification of additional novel KCC2 phosphorylation sites, kinases, and kinase regulators should drive future work on the roles of regulated KCC2 phosphorylation during CNS development and their contributions to GABA neurophysiology.

Materials and Methods

Immunoprecipitation and in-gel trypsin digestion of KCC2

Native mouse KCC2 was purified from brain lysates using 15μg rabbit anti-mouse KCC2 (Cat# 07–432, Millipore) conjugated to protein A agarose. In all cases, protein extracts were mixed with immunoprecipitating antibodies and incubated at 4 °C for 4 hours. IPs were washed and the products fractionated by SDS-PAGE on 4–20% gradient gels. Proteins of the expected molecular weights were visualized by QC colloidal Coomassie blue staining. The destained protein band was excised into 1 mm^3 pieces, which were then subjected to in-gel trypsin digestion. The gel pieces were washed with 1:1 acetonitrile (ACN):water followed by 1:1 ACN:NH_4HCO_3 (100 mM). Peptides produced by overnight trypsin digestion at 37°C were lyophilized for further analysis (25).

LC-MS/MS and quantitative analysis of KCC2 phosphorylation sites

Protein digests were analyzed using liquid chromatography–mass spectrometry (LC-MS/MS) on a Thermo Scientific Q Exactive Plus mass spectrometer equipped with a Waters nanoAcquity UPLC system utilizing a binary solvent system (Buffer A: 100% water, 0.1% formic acid; Buffer B: 100% acetonitrile, 0.1% formic acid). Trapping was performed at 5μl/min, 97% Buffer A for 3 min using a Waters Symmetry® C18 180μm x 20mm trap column. Peptides were separated using an ACQUITY UPLC PST (BEH) C18 nanoACQUITY Column 1.7 μm, 75 μm x 250 mm (37°C) and eluted at 300 nl/min with the following gradient: 3% buffer B at initial conditions; 5%−30% B in 140 min; 30%−50% B in 15 min; and 50%−90% B for 5–15 min before returning to initial conditions. Full MS scan was acquired in profile mode over the 300–1,500 m/z scan range using 1 microscan, 70,000 resolution, AGC target of 3E6, and a maximum injection time (IT) of 45 ms. Data-dependent MS/MS scan was acquired in centroid mode using 1 microscan, 17,500 resolution, AGC

target of 1E5, a maximum IT of 100 ms; 1.7 m/z isolation window; normalized collision energy of 28; and 200–2,000 m/z scan range. Up to 20 MS/MS scans were collected per MS scan on species with an intensity threshold of 1E4, charge states +2 to +6, peptide match preferred, and dynamic exclusion set to 20 seconds.

Raw mass spectra were searched against the mouse UniProt protein database using Andromeda search algorithm within MaxQuant 1.5.8.3 software (29, 77). Carbamidomethyl (C) was selected as a fixed modification, while oxidation (M), acetylation (protein N-term) and phosphorylation (STY) were selected as variable modifications. Perseus software 1.5.8.5 (78) was employed for quantitative analysis of the results from MaxQuant. The raw intensity of each phosphorylation site was normalized based on starting amount of proteins in the SDS-PAGE gel measured by densitometry. After removal of contaminant and reversed peptides, normalized phosphopeptide intensities were log2-transformed and filtered for valid values in 3 biological replicates from at least one developmental stage. Remaining missing values were imputed from the normal distribution. ANOVA with permutation-based FDR (control at 0.05) was used to detect significant differences in phosphopeptide levels between developmental stages. Hierarchical clustering of the z-score transformed abundance of the significant phosphorylation sites was performed using Euclidean distance and the average linkage method. Sequence logos around phosphorylated residues were created (PhosphoLogo) for subsets of significant sites based on profile plots (increasing or decreasing).

Construction of the Targeting Vector

The *Kcc2* gene-targeting vector was constructed from 129Sv mouse genomic DNA (Genoway, Lyon, France). T906E and T1007E point mutations were inserted into exon 22 and exon 24, respectively. A loxP-flanked Neomycin cassette was inserted in intron 22. Thr1007 corresponds to numbers in human and rat and the mutated residue in mouse is Thr1006. We mention this residue as Thr1007 in this paper to avoid confusion with previous studies performed using rat KCC2 and to be consistent with the mouse study by Moore *et al.* (2018).

Production of *Kcc2* double point mutant targeted ES cell clones

Linearized targeting vector was transfected into 129Sv ES cells (genOway, Lyon, France) according to genOway's electroporation procedures. PCR, Southern blot and sequence analysis of G-418 resistant ES clones revealed the recombined locus in 2 clones. PCR across the 5' end of the targeted locus used a forward primer hybridizing upstream of the 5' homology arm (5'- ATAGCGTTGGCTACCCGTGATATTGC-3') and a reverse primer hybridizing within the Neomycin cassette (5' AGGCTAGGCACAGGCTACATCCACAC-3'). Two Southern blot assays were hybridized with an internal and an external probe to assess recombination accuracy at the respective 5' and 3' ends of the *Kcc2* locus. Absence of off-target mutations was confirmed by sequence analysis.

Generation of chimeric mice and breeding scheme

Recombined ES cell clones microinjected into C57BL/6 blastocysts gave rise to male chimeras with significant ES cell contribution. These chimeras were bred with C57BL/6J mice expressing Cre-recombinase to produce the *Kcc2* double point mutant heterozygous line lacking the Neomycin cassette. F1 genotyping was performed by PCR and Southern blot. PCR primers hybridizing upstream (5'-GTGGTTCGCCTATGGGATCTGCTACTC-3') and down-stream (5'-AGACAAGGGTTCATGTAACAGACTCGCC-3') of the Neomycin cassette allowed PCR identification of the 298 bp *Kcc2* endogenous allele amplicon, the 1946 bp double point mutant allele ampicon harboring the Neomycin cassette, and the 387 bp double point mutant amplicon lacking the Neomycin cassette. Southern blot hybridization with an external probe allowed identification of the 14.1 kb wild-type allele and the 4.6 kb double point mutant allele.

Antibodies

The following antibodies were raised in sheep and affinity-purified on appropriate antigens by the Division of Signal Transduction Therapy Unit at the University of Dundee: KCC2A phospho-Thr 906 (SAYTYER(T)LMMEQRSRR [residues 975 – 989 of human KCC3A] corresponding to SAYTYEK(T)LVMEQRSQI [residues 899 – 915 of human KCC2A], S959C); KCC2A phospho-Thr 1007 (CYQEKVHM(T)WTKDKYM [residues 1032 – 1046 of human KCC3A] corresponding to TDPEKVHL(T)WTKDKSVA [residues 998 – 1014 of human KCC2A], S961C); NKCC1 total antibody [residues 1–288 of human NKCC1, S022D]; SPAK-total antibody [full-length GST-tagged human SPAK protein, S551D]; SPAK/OSR1 (S-motif) phospho-Ser373/Ser325 antibody [367–379 of human SPAK, RRVPGS(S)GHLHKT, which is highly similar to residues 319–331 of human OSR1 in which the sequence is RRVPGS(S)GRLHKT, S670B). Pan-KCC2 antibody (residues 932–1043 of human KCC2) was from NeuroMab (73–013). Anti (neuronal)-β-Tubulin III antibody was from Sigma-Aldrich (T8578). Horseradish peroxidase-coupled secondary antibodies used for immunoblotting were from Pierce. IgG for control immunoprecipitation experiments was affinity-purified from pre-immune serum using Protein G-Sepharose.

Buffers for Western Blots

Buffer A contained 50 mM Tris/HCl, pH 7.5 and 0.1mM EGTA. Lysis buffer was 50 mM Tris/HCl, pH 7.5, 1 mM EGTA, 1 mM EDTA, 50 mM sodium fluoride, 5 mM sodium pyrophosphate, 1 mM sodium orthovanadate, 1% (w/v) Triton-100, 0.27 M sucrose, 0.1% (v/v) 2-mercaptoethanol, and protease inhibitors (Roche complete protease inhibitor cocktail tablets, 1 tablet per 50 mL). Tris-buffered saline (TBS) -Tween buffer (TTBS) was Tris/HCl, pH 7.5, 0.15 M NaCl and 0.2% (v/v) Tween-20. SDS sample buffer was 1X NuPAGE LDS sample buffer (Invitrogen), containing 1% (v/v) 2-mercaptoethanol. Protein concentrations were determined following centrifugation of the lysate at 16,000 × g at 4 °C for 20 minutes using the Bradford method with bovine serum albumin as the standard.

Immunoprecipitation with phosphorylation site-specific antibodies

KCCs phosphorylated at KCC2 Thr906- and Thr1007-equivalent residues were immunoprecipitated from clarified hippocampal and cortical culture lysates (centrifuged at

16,000 × g at 4 °C for 20 minutes) using phosphorylation site-specific antibody coupled to protein G–Sepharose(19). The phosphorylation site-specific antibody was coupled with protein-G–Sepharose at a ratio of 1 mg of antibody per 1 mL of beads in the presence of 20 μg/mL lysate to which corresponding non-phosphorylated peptide had been added. Two mg clarified cell lysate were incubated with 15 μg antibody conjugated to 15 μL protein-G–Sepharose for 2 hours at 4°C with gentle agitation. Beads were washed three times with 1 mL of lysis buffer containing 0.15 M NaCl and twice with 1 mL of buffer A. Bound proteins were eluted with 1X LDS sample buffer.

Immunoblotting

Cell lysates (15 μg protein) in SDS sample buffer were subjected to electrophoresis on SDS-polyacrylamide gels and transferred to nitrocellulose membranes. The membranes were incubated for 30 min with TTBS containing 5% (w/v) skim milk, then immunoblotted in 5% (w/v) skim milk in TTBS with indicated primary antibodies overnight at 4°C. Antibodies prepared in sheep were used at concentrations of 1–2 μg/ml. The incubation with phosphorylation site-specific sheep antibodies was performed in the presence of 10 μg/mL of the non-phosphorylated form of the phosphorylated peptide antigen used to raise the antibody. The blots were then washed six times with TTBS and incubated for 1 hour at room temperature with secondary HRP-conjugated antibodies diluted 5000-fold in 5% (w/v) skim milk in TTBS. After repeating the washing steps, signal was detected with enhanced chemiluminescence reagent. Immunoblots were developed using a film automatic processor (SRX-101; Konica Minolta Medical) and films were scanned at 600-dpi resolution (PowerLook 1000; UMAX). Figures were generated with Photoshop and Illustrator (Adobe). The relative densitometry intensities of immunoblot bands were determined with ImageJ software.

Seizure induction by mild physiological stimulation

Seizures were induced in P0 mice by brushing, tail pinch, or tail suspension: For brushing, backs were brushed ten times with a soft brush. For tail pinch, tails were pinched with tweezers. For tail suspension, mice were suspended upside-down from their tails. Responses to stimulation were video-recorded for 300s and durations and types of seizures analyzed. Seizure severity was classified according to the presence or absence of opisthotonus.

Patch-clamp recordings from spinal cord neurons

The Animal Care and Use Committee of Hamamatsu University School of Medicine approved all animal experiments. All efforts were made to minimize the number of animals used and minimize suffering. Under deep isoflurane anesthesia, lumber spinal cords were removed from P0–1 mice and embedded in 3% agarose. Coronal lumber spinal cord slices (350 μm) were made using the vibrating microtome 7000 (Campden) in a cold, oxygenated sucrose solution containing (in mM): 220 sucrose, 120 NaCl, 2.5 KCl, 0.5 $CaCl_2$, 1.25 NaH_2PO_4, 1 $MgCl_2$, 26 $NaHCO_3$, 30 glucose, 10 $MgSO_4$ (pH 7.4). The slices were maintained in standard artificial cerebrospinal fluid (ACSF) consisting of (in mM) 120 NaCl, 2 KCl, 1 KH_2PO_4, 1 $MgCl_2$, 2 $CaCl_2$, 26 $NaHCO_3$, and 10 glucose (pH 7.4), and equilibrated with 95% O_2 and 5% CO_2 at room temperature prior to the recording. For recording, slices were transferred to a recording chamber, perfused with oxygenated ACSF

in the presence of tetrodotoxin (500 nM). Electrophysiological recordings were performed using a MultiClamp 700B amplifier (Molecular Devives) and pClamp9 software (Molecular Devives). Currents were filtered at 2 kHz, digitized at 10 kHz using DigiData1322A. The data were analyzed off-line using Clampfit9 (Molecular Devices).

To estimate the reversal potential of GABA-stimulated currents (E_{GABA}) in ventral spinal cord neurons in acute lumber slices, we performed gramicidin-perforated patch-clamp recording to acquire GABA-evoked responses with native intracellular Cl^- concentrations (9). Patch electrode pipettes (2–4 MΩ) were pulled from borosilicate glass capillaries on a P-97 puller (Sutter Instruments) and filled with pipette solution composed of 150 mM KCl and 10 mM HEPES (pH 7.2), supplemented with gramicidin. Gramicidin (Sigma-Aldrich) was dissolved in methanol to prepare a stock solution of 10 mg/ml, then diluted in pipette solution to a final concentration of 30 μg/ml.

Reversal potential of the 100 μM GABA-induced current was measured at −50 mV holding potential (V_h), and 0.5 s voltage ramps from −100 to 0 mV were applied before and during GABA application. E_{GABA} was estimated by measuring the voltage at which the I-V relationships before and during GABA application intersected (40). 30 sec duration GABA puffs were applied through a patch pipette approximated to the soma, using an IM-300 programmable microinjector (Narishige).

To measure the efficacy of KCC2 mediated Cl^- extrusion, we performed transient Cl^-loading by whole-cell voltage-clamp recording. Patch electrodes were filled with pipette solution containing (in mM) 123 K gluconate, 2 $MgCl_2$, 8 NaCl, 1 EGTA, 4 ATP, 0.3 GTP, and 10 HEPES (pH 7.2). Basal responses to 100 μM GABA puffs (3 psi and 3 sec duration) were recorded every 20 sec in current-clamp mode. Then, Cl^- was loaded by exposing the neurons to GABA for 20 sec in voltage-clamp mode (V_h=0 mV). After Cl^- loading, GABA responses were once again recorded every 20 sec in current-clamp mode to measure the rate of Cl^- extrusion (41).

Extracellular recordings from spinal cord ventral roots

For recordings of respiratory discharges, brainstem-spinal cord block preparations from P0 mice were isolated under deep isoflurane anesthesia (42). The brainstem was rostrally decerebrated between the VI cranial nerve roots and the lower border of the trapezoid body. The preparation was placed in a recording chamber and perfused continuously with the following modified ACSF (in mM): 124 NaCl, 5 KCl, 1.2 KH_2PO_4, 2.4 $CaCl_2$, 1.3 $MgSO_4$, 26 $NaHCO_3$, 30 glucose (pH 7.4), equilibrated with 95% O_2 and 5% CO_2. Respiratory motor neuron activity was recorded extracellularly with a glass suction electrode from the proximal end of ventral spinal roots at the cervical 4 (C4) or C5 level. The neuronal activity was recorded using a patch clamp amplifier (MultiClamp 700B) and pClamp9 software Neuronal activity (bursts per minute) was calculated from the mean burst activity over a period of 3 minutes.

For locomotor rhythm recording, spinal cord was isolated from P0–1 mice under deep isoflurane anesthesia (46). The spinal cord was dissected from the mid-cervical to sacral levels, placed in a recording chamber and perfused continuously with the following modified

ACSF (in mM): 118.4 NaCl, 4.69 KCl, 1.18 KH_2PO_4, 2.52 $CaCl_2$, 1.25 $MgSO_4$, 25 $NaHCO_3$, 11.1 glucose (pH 7.4), equilibrated with 95% O_2 and 5% CO_2. The locomotor rhythm (induced by perfusion with 20 μM 5-hydroxytryptamine (5-HT) (46)), was recorded from lumbar 2 (L2) ventral roots by suction electrode using a MultiClamp 700B amplifier. Data were sampled at 10 kHz, low-pass filtered at 3 kHz, high-pass filtered at 15 Hz and analyzed with pClamp9 software.

EdU staining

To label dividing cells, EdU (50 mg/kg/B.W., Invitrogen) was intraperitoneally injected into pregnant mice at E14.5. Under deep anesthesia with ketamine/xylazine, embryos were dissected at E18.5 and transcardially perfused with 4% paraformaldehyde. Brains were sectioned coronally (30 μm) and EdU was visualized using the Click-iT™ EdU Alexa Fluor 488 Imaging Kit (Invitorogen) according to manufacturer's protocol. Slices were imaged using a confocal laser-scanning microscope (FV1000-D; Olympus), and EdU positive cells were counted in coronal sections (3 sections of each animal) of the septum, preoptic area (POA), caudate-putamen (CPu), hippocampus (HP), and neocortex using Image J software (NIH).

Primary culture of neurons

E17.5 embryos (2 wild type and 2 homozygotes) were removed from pregnant mice under deep ketamine/xylazine anesthesia. Cortices were papain-dissociated for 20 min at 32 °C and plated on 10 mm microcoverglass (Matsunami) coated with polyethyleneimine in a Nunc 12-well dish (Thermo Fisher). One culture from each animal was maintained at 37 °C in Neurobasal medium (Invitrogen) supplemented with B-27 (Invitrogen), humidified 5% CO_2 / 95% air. Neurons were transfected with pCMV-EGFP at DIV (days in vitro) 5 using Lipofectamine 3000 (Invitrogen) per manufacturer's instructions. After 26 days in culture, neurons were fixed with 4% paraformaldehyde, permeabilized with 0.3% Triton X-100, then blocked with 1% normal goat serum and 2% bovine serum albumin. The neurons were then incubated overnight at 4°C with chicken anti-GFP antibody (1:500, Aves Labs). Goat anti-chicken AlexaFluor-conjugated secondary antibody (1:300, Invitrogen) was then applied for 2 h at room temperature. Immunofluorescent images were acquired by confocal laser-scanning microscope (FV1000-D; Olympus). Spine density was analyzed from 2 randomly selected neurons in each culture dish from individual animals by using the FilamentTracer module (v. 8.1.2, Bitplane) within Imaris software. Spine formation by WT and homozygote neurons were compared by unpaired t-tests.

Supplementary Material

Refer to Web version on PubMed Central for supplementary material.

Acknowledgments

Funding: K.T.K is supported by the March of Dimes, Simons Foundation, and National Institutes of Health (NIH) 4K12NS080223-05, RO1NS109358, and RO1NS111029. A.F. is supported by Grants-in-Aid for Scientific Research on Innovative Areas (#15H05872) from the Ministry of Education, Culture, Sports, Science and Technology of Japan and Grants-in-Aid for Scientific Research (B) #17H04025 from the Japan Society for the Promotion of Science.

References and Notes

1. Farrant M, and Kaila K. 2007 The cellular, molecular and ionic basis of GABA(A) receptor signalling. Progress in brain research 160: 59–87. [PubMed: 17499109]
2. Nakanishi K, Yamada J, Takayama C, Oohira A, and Fukuda A. 2007 NKCC1 activity modulates formation of functional inhibitory synapses in cultured neocortical neurons. Synapse (New York, N.Y 61: 138–149.
3. Wang DD, and Kriegstein AR. 2008 GABA regulates excitatory synapse formation in the neocortex via NMDA receptor activation. J Neurosci 28: 5547–5558. [PubMed: 18495889]
4. Haydar TF, Wang F, Schwartz ML, and Rakic P. 2000 Differential modulation of proliferation in the neocortical ventricular and subventricular zones. J Neurosci 20: 5764–5774. [PubMed: 10908617]
5. Behar TN, Schaffner AE, Scott CA, Greene CL, and Barker JL. 2000 GABA receptor antagonists modulate postmitotic cell migration in slice cultures of embryonic rat cortex. Cereb Cortex 10: 899–909. [PubMed: 10982750]
6. Cuzon VC, Yeh PW, Cheng Q, and Yeh HH. 2006 Ambient GABA promotes cortical entry of tangentially migrating cells derived from the medial ganglionic eminence. Cereb Cortex 16: 1377–1388. [PubMed: 16339085]
7. Bortone D, and Polleux F. 2009 KCC2 expression promotes the termination of cortical interneuron migration in a voltage-sensitive calcium-dependent manner. Neuron 62: 53–71. [PubMed: 19376067]
8. Rivera C, Voipio J, Payne JA, Ruusuvuori E, Lahtinen H, Lamsa K, Pirvola U, Saarma M, and Kaila K. 1999 The K+/Cl− co-transporter KCC2 renders GABA hyperpolarizing during neuronal maturation. Nature 397: 251–255. [PubMed: 9930699]
9. Yamada J, Okabe A, Toyoda H, Kilb W, Luhmann HJ, and Fukuda A. 2004 Cl- uptake promoting depolarizing GABA actions in immature rat neocortical neurones is mediated by NKCC1. The Journal of physiology 557: 829–841. [PubMed: 15090604]
10. Lu J, Karadsheh M, and Delpire E. 1999 Developmental regulation of the neuronal-specific isoform of K-Cl cotransporter KCC2 in postnatal rat brains. Journal of neurobiology 39: 558–568. [PubMed: 10380077]
11. Hubner CA, Stein V, Hermans-Borgmeyer I, Meyer T, Ballanyi K, and Jentsch TJ. 2001 Disruption of KCC2 reveals an essential role of K-Cl cotransport already in early synaptic inhibition. Neuron 30: 515–524. [PubMed: 11395011]
12. Kaila K, Price TJ, Payne JA, Puskarjov M, and Voipio J. 2014 Cation-chloride cotransporters in neuronal development, plasticity and disease. Nature reviews 15: 637–654.
13. Tiller NB, Price MJ, Campbell IG, and Romer LM. 2017 Effect of cadence on locomotor-respiratory coupling during upper-body exercise. Eur J Appl Physiol 117: 279–287. [PubMed: 28032253]
14. Ren J, and Greer JJ. 2003 Ontogeny of rhythmic motor patterns generated in the embryonic rat spinal cord. Journal of neurophysiology 89: 1187–1195. [PubMed: 12626606]
15. Wagner S, Castel M, Gainer H, and Yarom Y. 1997 GABA in the mammalian suprachiasmatic nucleus and its role in diurnal rhythmicity. Nature 387: 598–603. [PubMed: 9177347]
16. Silayeva L, Deeb TZ, Hines RM, Kelley MR, Munoz MB, Lee HH, Brandon NJ, Dunlop J, Maguire J, Davies PA, and Moss SJ. 2015 KCC2 activity is critical in limiting the onset and severity of status epilepticus. Proceedings of the National Academy of Sciences of the United States of America 112: 3523–3528. [PubMed: 25733865]
17. Stein V, Hermans-Borgmeyer I, Jentsch TJ, and Hubner CA. 2004 Expression of the KCl cotransporter KCC2 parallels neuronal maturation and the emergence of low intracellular chloride. The Journal of comparative neurology 468: 57–64. [PubMed: 14648690]
18. Delpy A, Allain AE, Meyrand P, and Branchereau P. 2008 NKCC1 cotransporter inactivation underlies embryonic development of chloride-mediated inhibition in mouse spinal motoneuron. The Journal of physiology 586: 1059–1075. [PubMed: 18096599]
19. Zhang J, Gao G, Begum G, Wang J, Khanna AR, Shmukler BE, Daubner GM, de Los Heros P, Davies P, Varghese J, Bhuiyan MI, Duan J, Zhang J, Duran D, Alper SL, Sun D, Elledge SJ, Alessi DR, and Kahle KT. 2016 Functional kinomics establishes a critical node of volume-sensitive

cation-Cl- cotransporter regulation in the mammalian brain. Scientific reports 6: 35986. [PubMed: 27782176]

20. Li H, Tornberg J, Kaila K, Airaksinen MS, and Rivera C. 2002 Patterns of cation-chloride cotransporter expression during embryonic rodent CNS development. The European journal of neuroscience 16: 2358–2370. [PubMed: 12492431]
21. Lee HH, Walker JA, Williams JR, Goodier RJ, Payne JA, and Moss SJ. 2007 Direct protein kinase C-dependent phosphorylation regulates the cell surface stability and activity of the potassium chloride cotransporter KCC2. The Journal of biological chemistry 282: 29777–29784. [PubMed: 17693402]
22. Lee HH, Jurd R, and Moss SJ. 2010 Tyrosine phosphorylation regulates the membrane trafficking of the potassium chloride co-transporter KCC2. Molecular and cellular neurosciences 45: 173–179. [PubMed: 20600929]
23. Rinehart J, Maksimova YD, Tanis JE, Stone KL, Hodson CA, Zhang J, Risinger M, Pan W, Wu D, Colangelo CM, Forbush B, Joiner CH, Gulcicek EE, Gallagher PG, and Lifton RP. 2009 Sites of regulated phosphorylation that control K-Cl cotransporter activity. Cell 138: 525–536. [PubMed: 19665974]
24. Friedel P, Kahle KT, Zhang J, Hertz N, Pisella LI, Buhler E, Schaller F, Duan J, Khanna AR, Bishop PN, Shokat KM, and Medina I. 2015 WNK1-regulated inhibitory phosphorylation of the KCC2 cotransporter maintains the depolarizing action of GABA in immature neurons. Science signaling 8: ra65. [PubMed: 26126716]
25. de Los Heros P, Alessi DR, Gourlay R, Campbell DG, Deak M, Macartney TJ, Kahle KT, and Zhang J. 2014 The WNK-regulated SPAK/OSR1 kinases directly phosphorylate and inhibit the K +-Cl− cotransporters. *The* Biochemical journal 458: 559–573. [PubMed: 24393035]
26. Inoue K, Furukawa T, Kumada T, Yamada J, Wang T, Inoue R, and Fukuda A. 2012 Taurine inhibits K+-Cl− cotransporter KCC2 to regulate embryonic Cl- homeostasis via with-no-lysine (WNK) protein kinase signaling pathway. The Journal of biological chemistry 287: 20839–20850. [PubMed: 22544747]
27. Heubl M, Zhang J, Pressey JC, Al Awabdh S, Renner M, Gomez-Castro F, Moutkine I, Eugene E, Russeau M, Kahle KT, Poncer JC, and Levi S. 2017 GABAA receptor dependent synaptic inhibition rapidly tunes KCC2 activity via the Cl(−)-sensitive WNK1 kinase. Nature communications 8: 1776.
28. Sedmak G, Jovanov-Milosevic N, Puskarjov M, Ulamec M, Kruslin B, Kaila K, and Judas M. 2016 Developmental Expression Patterns of KCC2 and Functionally Associated Molecules in the Human Brain. Cereb Cortex 26: 4574–4589. [PubMed: 26428952]
29. Cox J, and Mann M. 2008 MaxQuant enables high peptide identification rates, individualized p.p.b.-range mass accuracies and proteome-wide protein quantification. Nature biotechnology 26: 1367–1372.
30. Sharma K, D'Souza RC, Tyanova S, Schaab C, Wisniewski JR, Cox J, and Mann M. 2014 Ultradeep human phosphoproteome reveals a distinct regulatory nature of Tyr and Ser/Thr-based signaling. Cell reports 8: 1583–1594. [PubMed: 25159151]
31. Faresse N, Vitagliano JJ, and Staub O. 2012 Differential ubiquitylation of the mineralocorticoid receptor is regulated by phosphorylation. FASEB J 26: 4373–4382. [PubMed: 22798426]
32. Hornbeck PV, Zhang B, Murray B, Kornhauser JM, Latham V, and Skrzypek E. 2015 PhosphoSitePlus, 2014: mutations, PTMs and recalibrations. Nucleic acids research 43: D512–520. [PubMed: 25514926]
33. Kahle KT, Schmouth JF, Lavastre V, Latremoliere A, Zhang J, Andrews N, Omura T, Laganiere J, Rochefort D, Hince P, Castonguay G, Gaudet R, Mapplebeck JC, Sotocinal SG, Duan J, Ward C, Khanna AR, Mogil JS, Dion PA, Woolf CJ, Inquimbert P, and Rouleau GA. 2016 Inhibition of the kinase WNK1/HSN2 ameliorates neuropathic pain by restoring GABA inhibition. Science signaling 9: ra32. [PubMed: 27025876]
34. Moore YE, Deeb TZ, Chadchankar H, Brandon NJ, and Moss SJ. 2018 Potentiating KCC2 activity is sufficient to limit the onset and severity of seizures. Proceedings of the National Academy of Sciences of the United States of America 115: 10166–10171. [PubMed: 30224498]

35. Kahle KT, Khanna AR, Duan J, Staley KJ, Delpire E, and Poduri A. 2016 The KCC2 Cotransporter and Human Epilepsy: Getting Excited About Inhibition. Neuroscientist 22: 555–562. [PubMed: 27130838]
36. Ben-Ari Y, Khalilov I, Kahle KT, and Cherubini E. 2012 The GABA excitatory/inhibitory shift in brain maturation and neurological disorders. Neuroscientist 18: 467–486. [PubMed: 22547529]
37. Li H, Khirug S, Cai C, Ludwig A, Blaesse P, Kolikova J, Afzalov R, Coleman SK, Lauri S, Airaksinen MS, Keinanen K, Khiroug L, Saarma M, Kaila K, and Rivera C. 2007 KCC2 interacts with the dendritic cytoskeleton to promote spine development. Neuron 56: 1019–1033. [PubMed: 18093524]
38. Boulenguez P, Liabeuf S, Bos R, Bras H, Jean-Xavier C, Brocard C, Stil A, Darbon P, Cattaert D, Delpire E, Marsala M, and Vinay L. 2010 Down-regulation of the potassium-chloride cotransporter KCC2 contributes to spasticity after spinal cord injury. Nature medicine 16: 302–307.
39. Watanabe M, and Fukuda A. 2015 Development and regulation of chloride homeostasis in the central nervous system. Frontiers in cellular neuroscience 9: 371. [PubMed: 26441542]
40. Saitsu H, Watanabe M, Akita T, Ohba C, Sugai K, Ong WP, Shiraishi H, Yuasa S, Matsumoto H, Beng KT, Saitoh S, Miyatake S, Nakashima M, Miyake N, Kato M, Fukuda A, and Matsumoto N. 2016 Impaired neuronal KCC2 function by biallelic SLC12A5 mutations in migrating focal seizures and severe developmental delay. Scientific reports 6: 30072. [PubMed: 27436767]
41. Ellender TJ, Raimondo JV, Irkle A, Lamsa KP, and Akerman CJ. 2014 Excitatory effects of parvalbumin-expressing interneurons maintain hippocampal epileptiform activity via synchronous afterdischarges. J Neurosci 34: 15208–15222. [PubMed: 25392490]
42. Fujii M, Arata A, Kanbara-Kume N, Saito K, Yanagawa Y, and Obata K. 2007 Respiratory activity in brainstem of fetal mice lacking glutamate decarboxylase 65/67 and vesicular GABA transporter. Neuroscience 146: 1044–1052. [PubMed: 17418495]
43. Guertin PA 2009 The mammalian central pattern generator for locomotion. Brain research reviews 62: 45–56. [PubMed: 19720083]
44. Zhang J, Lanuza GM, Britz O, Wang Z, Siembab VC, Zhang Y, Velasquez T, Alvarez FJ, Frank E, and Goulding M. 2014 V1 and v2b interneurons secure the alternating flexor-extensor motor activity mice require for limbed locomotion. Neuron 82: 138–150. [PubMed: 24698273]
45. Nishimaru H, and Kudo N. 2000 Formation of the central pattern generator for locomotion in the rat and mouse. Brain research bulletin 53: 661–669. [PubMed: 11165801]
46. Nishimaru H, Takizawa H, and Kudo N. 2000 5-Hydroxytryptamine-induced locomotor rhythm in the neonatal mouse spinal cord in vitro. Neuroscience letters 280: 187–190. [PubMed: 10675792]
47. Horn Z, Ringstedt T, Blaesse P, Kaila K, and Herlenius E. 2010 Premature expression of KCC2 in embryonic mice perturbs neural development by an ion transport-independent mechanism. The European journal of neuroscience 31: 2142–2155. [PubMed: 20529123]
48. Awad PN, Amegandjin CA, Szczurkowska J, Carrico JN, Fernandes do Nascimento AS, Baho E, Chattopadhyaya B, Cancedda L, Carmant L, and Di Cristo G. 2018 KCC2 Regulates Dendritic Spine Formation in a Brain-Region Specific and BDNF Dependent Manner. Cereb Cortex 28: 4049–4062. [PubMed: 30169756]
49. Branchereau P, Chapron J, and Meyrand P. 2002 Descending 5-hydroxytryptamine raphe inputs repress the expression of serotonergic neurons and slow the maturation of inhibitory systems in mouse embryonic spinal cord. J Neurosci 22: 2598–2606. [PubMed: 11923425]
50. Sibilla S, and Ballerini L. 2009 GABAergic and glycinergic interneuron expression during spinal cord development: dynamic interplay between inhibition and excitation in the control of ventral network outputs. Progress in neurobiology 89: 46–60. [PubMed: 19539686]
51. Ritter B, and Zhang W. 2000 Early postnatal maturation of GABAA-mediated inhibition in the brainstem respiratory rhythm-generating network of the mouse. The European journal of neuroscience 12: 2975–2984. [PubMed: 10971638]
52. Brockhaus J, and Ballanyi K. 1998 Synaptic inhibition in the isolated respiratory network of neonatal rats. The European journal of neuroscience 10: 3823–3839. [PubMed: 9875360]
53. Johnson SM, Smith JC, and Feldman JL. 1996. Modulation of respiratory rhythm in vitro: role of Gi/o protein-mediated mechanisms. J Appl Physiol *(*1985*)* 80: 2120–2133.

54. Shao XM, and Feldman JL. 1997 Respiratory rhythm generation and synaptic inhibition of expiratory neurons in pre-Botzinger complex: differential roles of glycinergic and GABAergic neural transmission. Journal of neurophysiology 77: 1853–1860. [PubMed: 9114241]
55. Haji A, Takeda R, and Remmers JE. 1992 Evidence that glycine and GABA mediate postsynaptic inhibition of bulbar respiratory neurons in the cat. J Appl Physiol (1985) 73: 2333–2342. [PubMed: 1337074]
56. Champagnat J, Denavit-Saubie M, Moyanova S, and Rondouin G. 1982 Involvement of amino acids in periodic inhibitions of bulbar respiratory neurones. Brain research 237: 351–365. [PubMed: 6123370]
57. Haji A, Takeda R, and Okazaki M. 2000 Neuropharmacology of control of respiratory rhythm and pattern in mature mammals. Pharmacol Ther 86: 277–304. [PubMed: 10882812]
58. Schmid K, Foutz AS, and Denavit-Saubie M. 1996 Inhibitions mediated by glycine and GABAA receptors shape the discharge pattern of bulbar respiratory neurons. Brain research 710: 150–160. [PubMed: 8963654]
59. Yajima Y, and Hayashi Y. 1999 Ambiguous respiratory neurons are modulated by GABA(A) receptor-mediated inhibition. Neuroscience 90: 249–257. [PubMed: 10188951]
60. Ren J, Momose-Sato Y, Sato K, and Greer JJ. 2006 Rhythmic neuronal discharge in the medulla and spinal cord of fetal rats in the absence of synaptic transmission. Journal of neurophysiology 95: 527–534. [PubMed: 16148265]
61. Okabe A, Shimizu-Okabe C, Arata A, Konishi S, Fukuda A, and Takayama C. 2015 KCC2-mediated regulation of respiration-related rhythmic activity during postnatal development in mouse medulla oblongata. Brain research 1601: 31–39. [PubMed: 25596421]
62. Wang C, Shimizu-Okabe C, Watanabe K, Okabe A, Matsuzaki H, Ogawa T, Mori N, Fukuda A, and Sato K. 2002 Developmental changes in KCC1, KCC2, and NKCC1 mRNA expressions in the rat brain. Brain research 139: 59–66. [PubMed: 12414094]
63. Fukuda A, Nakanishi Y, Kumada T, and Furukawa T. 2013 Multimodal GABAA receptor functions on cell development In Comprehensive Developmental Neuroscience: Cellular Migration and Formation of Neuronal Connections. Rubenstein JLR, and Rakic P, eds. Elsevier, Amsterdam 921–939.
64. Khirug S, Ahmad F, Puskarjov M, Afzalov R, Kaila K, and Blaesse P. 2010 A single seizure episode leads to rapid functional activation of KCC2 in the neonatal rat hippocampus. J Neurosci 30: 12028–12035. [PubMed: 20826666]
65. Mavrovic M, Uvarov P, Vutskits L, Puskarjov M, and Kaila K. 2018 KCC2 regulates migration of pyramidal neurons in the developing mouse neocortex in an ion transport-independent manner. In 11th FENS Forum of Neuroscience, Berlin, Germany.
66. Hoerder-Suabedissen A, and Molnar Z. 2015 Development, evolution and pathology of neocortical subplate neurons. Nature reviews 16: 133–146.
67. Achilles K, Okabe A, Ikeda M, Shimizu-Okabe C, Yamada J, Fukuda A, Luhmann HJ, and Kilb W. 2007 Kinetic properties of Cl uptake mediated by Na+-dependent K+−2Cl cotransport in immature rat neocortical neurons. J Neurosci 27: 8616–8627. [PubMed: 17687039]
68. Sloviter RS 1991 Permanently altered hippocampal structure, excitability, and inhibition after experimental status epilepticus in the rat: the “dormant basket cell” hypothesis and its possible relevance to temporal lobe epilepsy. Hippocampus 1: 41–66. [PubMed: 1688284]
69. Naylor DE, Liu H, and Wasterlain CG. 2005 Trafficking of GABA(A) receptors, loss of inhibition, and a mechanism for pharmacoresistance in status epilepticus. J Neurosci 25: 7724–7733. [PubMed: 16120773]
70. Isomura Y, Sugimoto M, Fujiwara-Tsukamoto Y, Yamamoto-Muraki S, Yamada J, and Fukuda A. 2003 Synaptically activated Cl- accumulation responsible for depolarizing GABAergic responses in mature hippocampal neurons. Journal of neurophysiology 90: 2752–2756. [PubMed: 14534278]
71. Deeb TZ, Nakamura Y, Frost GD, Davies PA, and Moss SJ. 2013 Disrupted Cl(−) homeostasis contributes to reductions in the inhibitory efficacy of diazepam during hyperexcited states. The European journal of neuroscience 38: 2453–2467. [PubMed: 23627375]

72. Fujiwara-Tsukamoto Y, Isomura Y, Nambu A, and Takada M. 2003 Excitatory GABA input directly drives seizure-like rhythmic synchronization in mature hippocampal CA1 pyramidal cells. Neuroscience 119: 265–275. [PubMed: 12763087]

73. Kelley MR, Deeb TZ, Brandon NJ, Dunlop J, Davies PA, and Moss SJ. 2016 Compromising KCC2 transporter activity enhances the development of continuous seizure activity. Neuropharmacology 108: 103–110. [PubMed: 27108931]

74. Kaila K 1994 Ionic basis of GABAA receptor channel function in the nervous system. Progress in neurobiology 42: 489–537. [PubMed: 7522334]

75. Doyon N, Prescott SA, Castonguay A, Godin AG, Kroger H, and De Koninck Y. 2011 Efficacy of synaptic inhibition depends on multiple, dynamically interacting mechanisms implicated in chloride homeostasis. PLoS computational biology 7: e1002149. [PubMed: 21931544]

76. Sato A, and Shibuya H. 2018 Glycogen synthase kinase 3 beta functions as a positive effector in the WNK signaling pathway. PloS one 13.

77. Cox J, Neuhauser N, Michalski A, Scheltema RA, Olsen JV, and Mann M. 2011 Andromeda: A Peptide Search Engine Integrated into the MaxQuant Environment. J Proteome Res 10: 1794–1805. [PubMed: 21254760]

78. Tyanova S, Temu T, Sinitcyn P, Carlson A, Hein MY, Geiger T, Mann M, and Cox J. 2016 The Perseus computational platform for comprehensive analysis of (prote)omics data. Nat Methods 13: 731–740. [PubMed: 27348712]

79. Weber M, Hartmann AM, Beyer T, Ripperger A, and Nothwang HG. 2014 A novel regulatory locus of phosphorylation in the C terminus of the potassium chloride cotransporter KCC2 that interferes with N-ethylmaleimide or staurosporine-mediated activation. The Journal of biological chemistry 289: 18668–18679. [PubMed: 24849604]

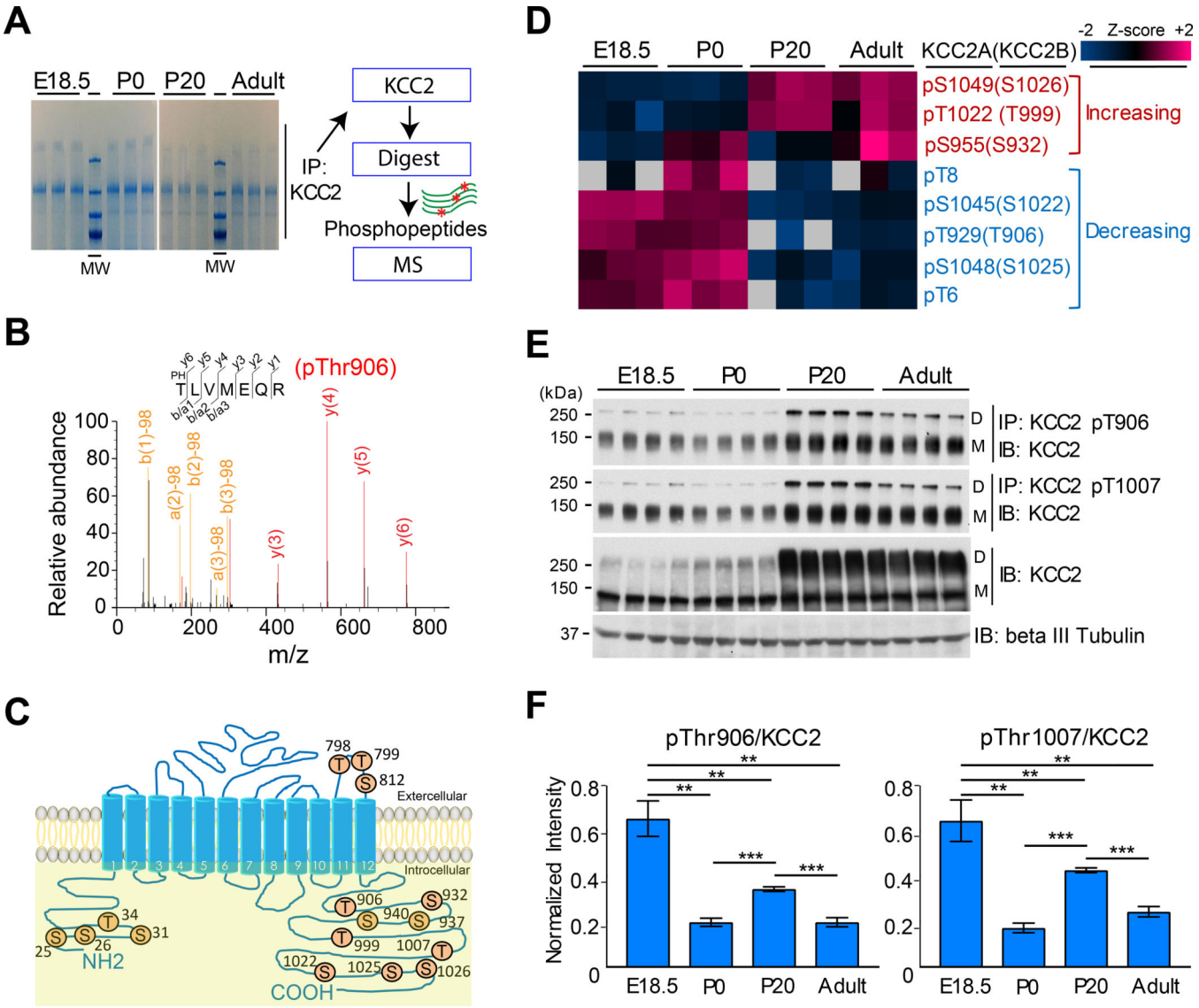

Figure 1. Identification of KCC2 phosphorylation sites regulated during CNS development.

(A) Phosphorylation site mapping. KCC2 was immunopurified from mouse brain, fractionated by SDS-PAGE, and digested with trypsin. Blot is representative of lysates from 19 mice. Schematic lays out how phospho-peptides were subjected to LC-MS/MS. **(B)** Representative MS/MS spectrum assignment of peptide TLVMEQR (pThr^{929}; presented as human KCC2B pThr^{906}). The phosphorylated precursor ion (478.71 +2) was selected and produced the fragment ion spectrum shown. Specific y and b fragment ions allowed unambiguous identification of the precursor peptide and its phosphorylation at Thr^{906} (human numbering). Fragment ions with neutral loss of phosphate (-Pb/a1, -Pb/a2, -Pb/a3 etc.) are indicated. **(C)** Identified KCC2 phosphorylation sites are numbered as in human KCC2B (GeneID 57468). All KCC2 peptides observed at various developmental stages are listed in table S1. **(D)** Heat map representation of significant KCC2 phosphorylation sites and their changes during development. Hierarchical clustering showed distinct pattern of KCC2 phosphorylation at these residues. Amino acid residue numbering is referenced to

isoform 1 of mouse *Slc12a5* (UniProt: Q91V14). **(E)** Brain lysates were subjected to immunoprecipitation (IP) by pan-KCC2 antibody (KCC2) or by phosphorylation site-specific antibodies recognizing the Thr^{906}- or Thr^{1007}-phosphorylated forms of KCC2, and immuno-precipitated protein was detected with pan-KCC2 antibody (IB). Whole-cell lysates were subjected to immunoblot using antibodies recognizing the indicated proteins or phosphoproteins. D, dimeric KCC2; M, monomeric KCC2. Blot is representative of 3 experiments. **(F)** Band intensities represented in (E) were quantitated with ImageJ software. Calculation of intensity ratios was based on the calculation: (phospho-dimeric KCC2 + phospho-monomeric KCC2) / (total dimeric KCC2 + total monomeric KCC2), as described previously (24). ***p<0.001; **p<0.01; *p<0.05; ns, not significant by one-way ANOVA with *post-hoc* testing (n=6, data are mean ± SEM).

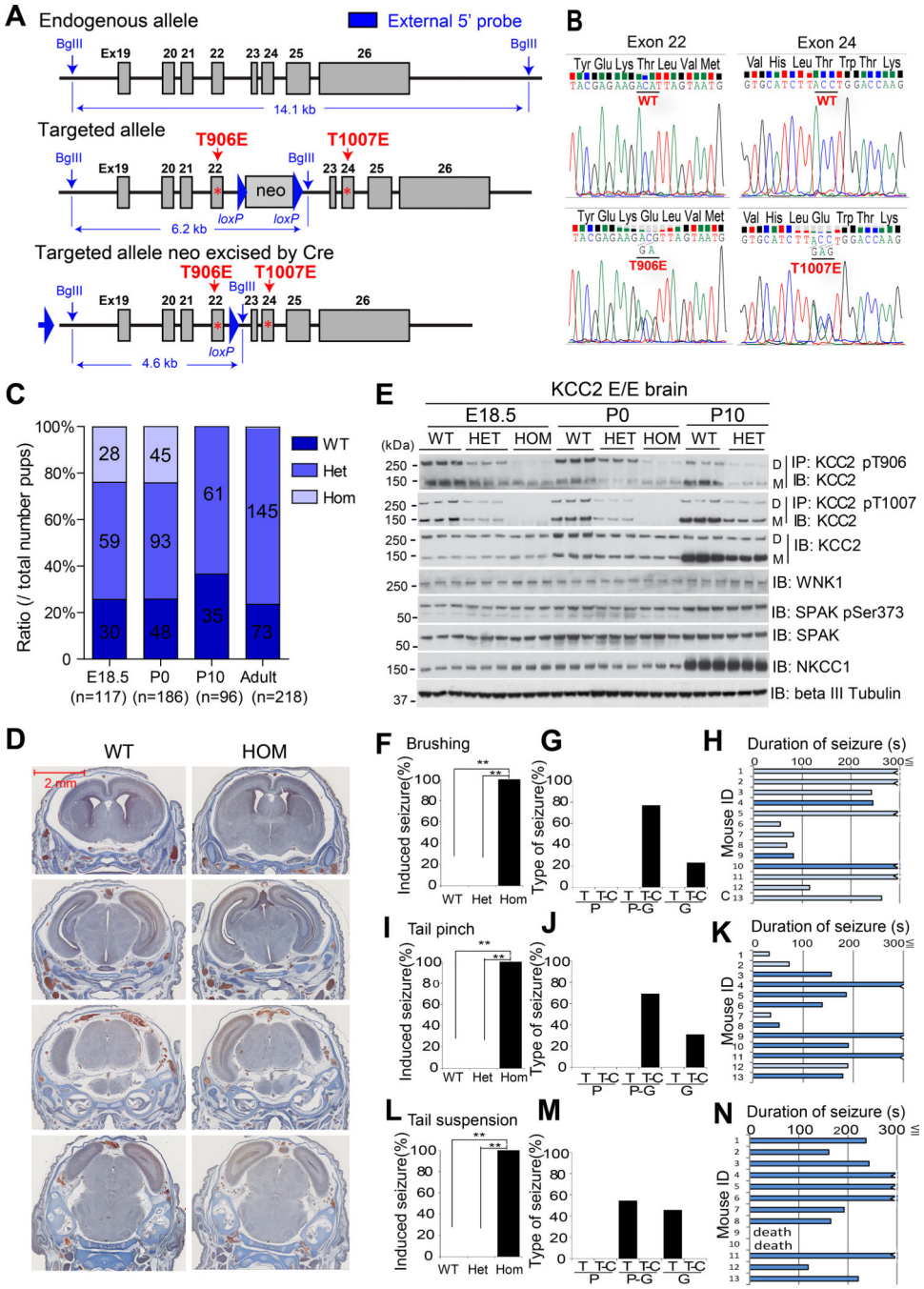

Figure 2. KCC2 T906E/T1007E (*Kcc2*$^{E/E}$) phospho-mimetic mice.

(A) Genomic targeting strategy depicting T906E (exon 22) and T1007E (exon 24). The intron 22 Neomycin selection cassette is excised by Cre recombinase. **(B)** Sanger sequencing trace of KCC2 T906E/T1007E. **(C)** Genotypes of surviving progeny from *Kcc2*$^{+/E}$ intercrosses at E18.5, P0, and P10. N is noted in the graph. **(D)** Consecutive axial brain sections revealed no gross defects in *Kcc2*$^{E/E}$ mutant mice (hom, p0). Images are representative of 20 mice. **(E)** WT brain lysates at indicated ages were immunoprecipitated (IP) with site-specific phospho-antibodies recognizing KCC2 pThr^{906} or pThr^{1007}.

Immunoprecipitates were immunoblotted with pan-KCC2 antibody (IB). Whole-cell lysates were immunoblotted with indicated antibodies. D, dimeric KCC2; M, monomeric KCC2. Band intensities were quantitated with ImageJ software, shown in fig. S2C. Blot is representative of 3 experiments. **(F to N)** Percentage of WT, heterozygous (het) and homozygous (hom) P0 *Kcc2*$^{E/E}$ mice exhibiting seizures, type of seizure [partial (P), secondary generalized (G), tonic (T), and tonic-clonic types (T-C)], and duration of seizure (with or without opisthotonos: dark and light blue, respectively) provoked by brushing (F to H), tail pinch (I to K), and tail suspension (L to N). **$p<0.01$ by chi square test. Data are from 11–13 mice.

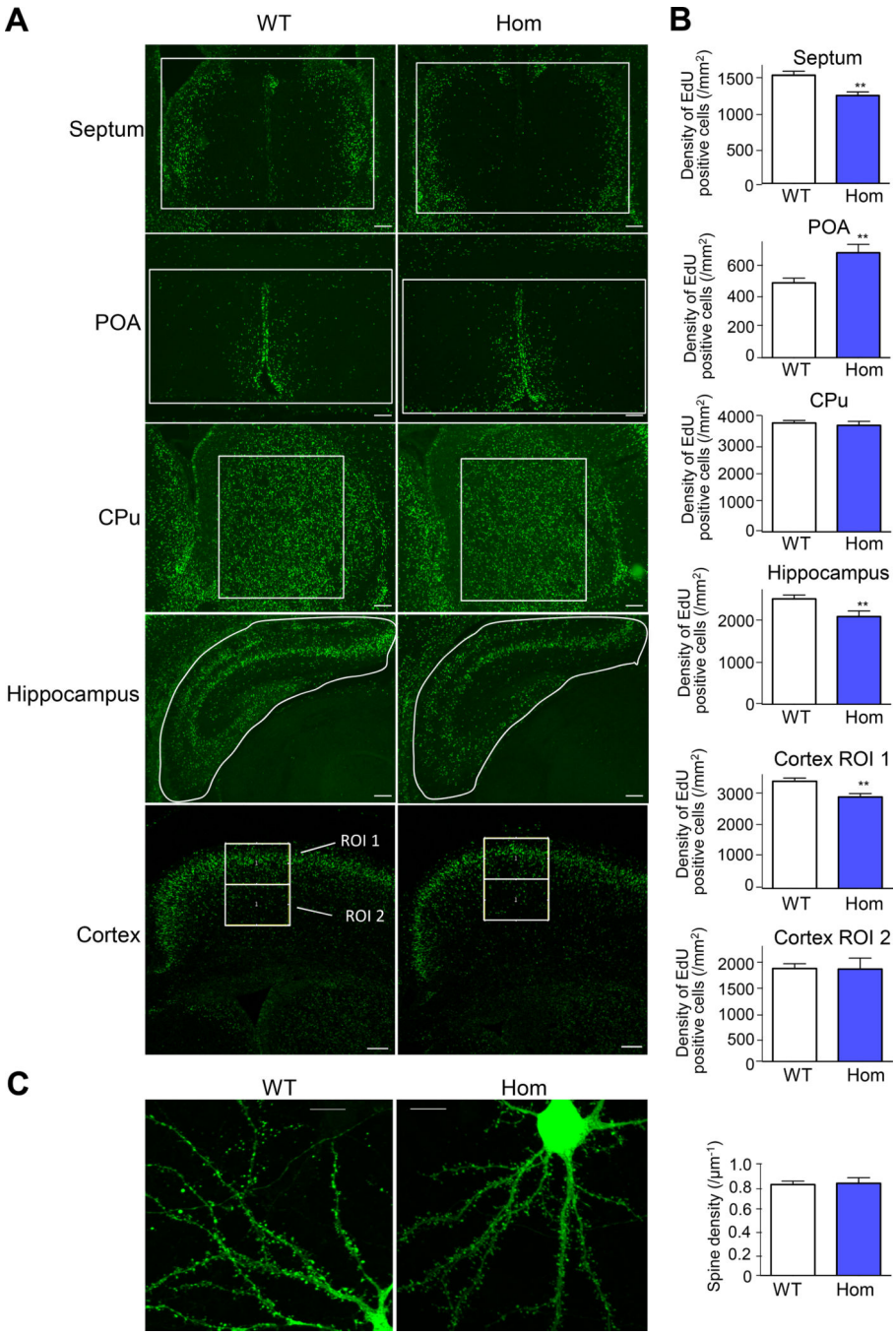

Figure 3. Developing *Kcc2*$^{E/E}$ mouse brains exhibit anomalous distribution of proliferating neurons but normal dendritic spine morphology.

(A) Neuronal distribution in WT and homozygous *Kcc2*$^{E/E}$ E14.5 brains. Representative images of EdU-positive neurons in the septum, hypothalamus, hippocampus, and cortex of WT (n = 3) and homozygous *Kcc2*$^{E/E}$ (n = 4) mouse brains. Proliferating cells were labeled with EdU at E14.5 and then immunostained for EdU at E18.5. EdU-positive cells in each region of interest (ROI) were counted as in Methods. Images are representative of 7 mice. **(B)** Quantitation of EdU-positive neuron density in WT versus homozygous *Kcc2*$^{E/E}$ E14.5

brains, assessed in the septum, pre-optic area (POA), caudate-putamen (CPu), hippocampus, and cortex (ROI 1 and 2). **p<0.01 by unpaired t-test, n=4 (*Kcc2*$^{E/E}$) and 3 (WT). **(C)** Spine formation in WT and homozygous *Kcc2*$^{E/E}$ neurons. Representative images of EGFP-transfected DIV 26 primary cultured cortical neurons from WT and homozygous *Kcc2*$^{E/E}$ mice (each n=3).

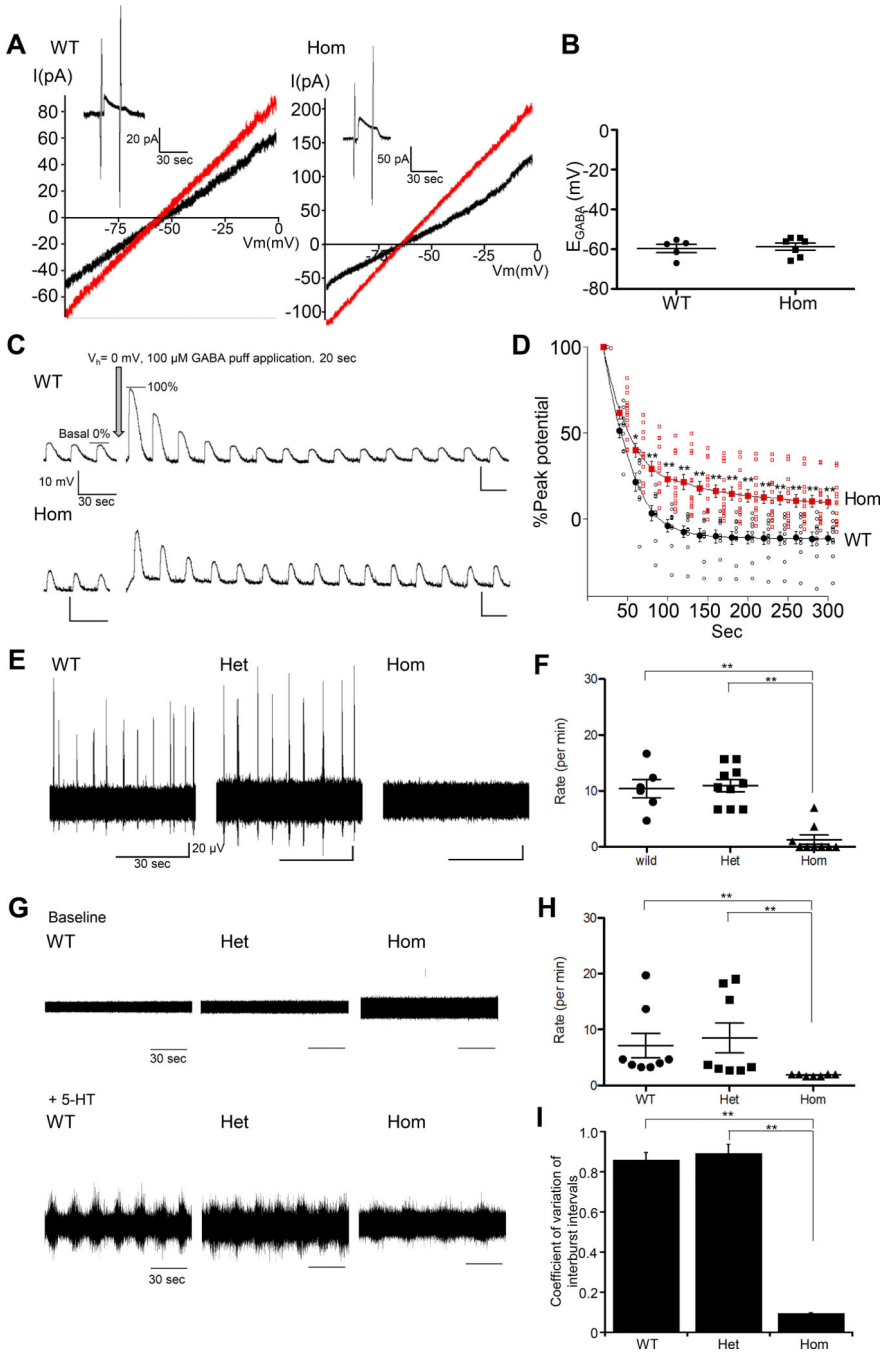

Figure 4. *Kcc2*$^{E/E}$ neurons exhibit impaired GABA-dependent Cl^- extrusion, and disrupted rhythmogenesis.

(A) Gramicidin-perforated, voltage-clamped currents (9) recorded at −50 mV holding potential. Two 0.5 s voltage ramps from −100 to 0 mV were applied before and during 30 s puff application of 100 µM GABA; sample I-V curves before (black) and after GABA application (red). E_{GABA} was estimated from the voltage axis intercept (detailed further in the Methods). Insets (upper left) are representative GABA-evoked current traces at −50 mV holding potential in ventral spinal cord neurons of acute lumber spinal cord slices from P0 WT (left) and *Kcc2*$^{E/E}$ mice (right). Data are representative of 12 mice. **(B)** Neuronal E_{GABA}

from WT (−59.6 ± 2.1; n=5) and homozygous *Kcc2*$^{E/E}$ mice (−58.7 ± 1.8 mV; n=7). Data were not significantly different by an unpaired t-test. **(C)** Representative traces of GABA responses in P0 ventral spinal cord neurons of acute lumber spinal cord slices from WT and *Kcc2*$^{E/E}$ mice. After current clamp recording of basal GABA responses (3-s 100 μM GABA puffs every 20 s) in neurons from WT and *Kcc2*$^{E/E}$ mice, neurons were Cl^--loaded by prolonged (20 s) GABA puff during depolarizing voltage-clamp (Vh = 0 mV). Post-Cl^--loading, responses to brief GABA puffs were again recorded in current-clamp mode, demonstrating 407±78% increased peak neuronal Cl^- extrusion. Data are representative of 23 mice. **(D)** Normalized recovery of neuronal GABA responses in WT (black circles; n=10) and *Kcc2*$^{E/E}$ mice (red squares; n=13) post-Cl^- loading. Cl^- extrusion rate was impaired in *Kcc2*$^{E/E}$ mice. Each neuronal response was normalized to the GABA pulse peak value (0%) and to peak post-Cl^- loading GABA pulse-induced response (100%) for each neuron. WT peak potentials recovered to initial values (−3.9 ± 3.8%; n=10), whereas *Kcc2*$^{E/E}$ peak potentials remained 23.0 ± 4.1% above initial values (n=13). *p<0.05, **p<0.01 by unpaired t-test. Open symbols, single cells; filled symbols, mean values with standard error. **(E)** Respiratory motor neuron recordings from P0 mouse cervical spinal cord ventral rootlets (C4-C5) (42). Spontaneous rhythmic activity was measured in WT mice (n=6), *T906E/T1007E*$^{+/wt}$ mice (n=10), and *Kcc2*$^{E/E}$ mice (n=11). **(F)** Respiratory rhythm of WT (10.4 ± 1.1 min^{-1}; n=6), heterozygous *Kcc2*$^{E/wt}$ (11 ± 1.1 min^{-1}; n=10), and *Kcc2*$^{E/E}$ mice (1.3 ± 0.8 min^{-1}; n=9). Means ± SEM; **p<0.01 by Kruskal-Wallis test. **(G)** P0 L2 ventral root spontaneous activity (upper traces), and locomotor rhythm (lower traces) was induced by perfusion of 20 μM 5-HT (45, 46) in WT (n=8), heterozygous (n=8), and *Kcc2*$^{E/E}$ mice (n=7). **(H)** Rate of the locomotor rhythm in WT (7.1 ± 2.2 min^{-1}; n=8), *T906E/T1007E*$^{+/wt}$ mice (8.5 ± 2.7 min^{-1}; n=8), and *Kcc2*$^{E/E}$ mice (1.9 ± 0.1 min^{-1}; n=7). Means ± SEM; **p<0.01 by Kruskal-Wallis test. **(I)** Coefficient of variation of interburst intervals in WT (0.9 ± 0.04; n=8), *T906E/T1007E*$^{+/wt}$ mice (0.9 ± 0.04; n=8), and *Kcc2*$^{E/E}$ mice (0.1 ± 0.001; n=7). Means ± SEM; **p<0.01 by Kruskal-Wallis test.